THE PUBLISHING HOUSE
OF THE ROMANIAN ACADEMY

PROCEEDINGS OF THE ROMANIAN ACADEMY, Series A,
Volume 14, Number 4/2013, pp. 317–325

PUMP INDUCER OPTIMIZATION BASED ON CAVITATION CRITERION

Irina Georgeta MOISĂ[1], Romeo SUSAN-RESIGA[1], Sebastian MUNTEAN[2]

[1] "Politehnica" University of Timişoara, Romania
[2] Center of Advanced Research in Engineering Sciences, Romanian Academy - Timişoara Branch, Romania
E-mail: resiga@mh.mec.upt.ro

The paper presents the optimization procedure of a pump inducer taking into account the cavitation criterion. The pump inducer optimization procedure is based on inverse design method where the inflow and outflow conditions are known. Axial flow is considered as upstream condition while the downstream swirling flow is suited for the pump impeller inlet, respectively. The key ingredient in this procedure is the function of loading shape which provides the distribution of blade loading from leading edge to trailing edge. A new parametric analytical expression is introduced in this paper for the loading shape function. The objective function corresponds to the minimum pressure coefficient with reverse sign, which is minimized within the chosen parameter space. This procedure is applied for optimize a pump inducer with three blades, with improved cavitating performance.

Key words: pump inducer, inverse design method, cavitational optimization.

1. INTRODUCTION

Nowadays, pumping systems account for nearly 20% of the world's electrical energy demand and range from 25–50% of the energy usage in certain industrial plant operations [1]. The pumping systems are widely used in industry to store energy, to provide cooling and lubrication services, to transfer fluids for processing, and to provide the driving force in hydraulic systems. Clearly, pumping systems consume a significant amount of the total electrical energy. The key element of the pumping system is the pumping unit which includes the electrical motor and the hydraulic pump. In the manufacturing sector, pumps represent 27% of the electricity used by industrial systems [2]. As a result, the improvements of energetic and cavitational performances of the pumps become more and more important. A common technical solution is to install an inducer at the pump impeller inlet in order to improve the cavitational behavior of the pumps [3]. Generally, inducers are axial flow impellers with a small blade numbers and long blades. As a result, an inducer increases the inlet static pressure at the impeller inlet thus improving the overall cavitational performances. Using conventional design the inducers blades with helical surfaces and a straight line or a combination of straight lines and curves is chosen for the camber line [4]. The extensive experimental and numerical investigations have been performed in our group in order to improve the performances of these inducers during last two decades [4–6]. However, the inducer design guidelines are based on the empirical relationship between geometry parameters and performance characteristics [7]. Moreover, the designed inducers based on conventional methods may have leading edge backflow even at the design point. Therefore, the three-dimensional inverse design method developed by Zangeneh et al. [8] was applied to improve the inlet backflow characteristics of highly loaded turbopump inducers for a liquid hydrogen rocket engine [9]. Optimizing the blade loading distribution using the three-dimensional inverse design method eliminates this inlet backflow [10]. Consequently, the numerical and experimental investigations were performed in order to compare the performance of inducers with different blade loadings, [11].

In situ experimental investigations performed by Anton [12] on large double suction storage pumps have revealed serious cavitational problems. As a result, a model inducer (Fig. 1) was designed using inverse design method [13] based on the technical specifications shown in Table 1. The loading function $\partial(rv_u)/\partial x$ imposed along to three sections of the blade: S_H near the hub, S_M in the middle and S_T near the tip and

dimensionless loading (rv_u), along the leading and trailing edges are plotted against normalized abscissa x^* in Figs. 2 and 3, respectively.

Table 1

Design specifications for inducer

Rotation speed n [rpm]	2900
Tip diameter $D_T = D_{ref} = 2R_{ref}$ [mm]	103
Hub diameter D_H [mm]	40
Blade number Z [-]	3
Blade thicknes t [mm]	3
Design flow rate Q [l/s]	40.2

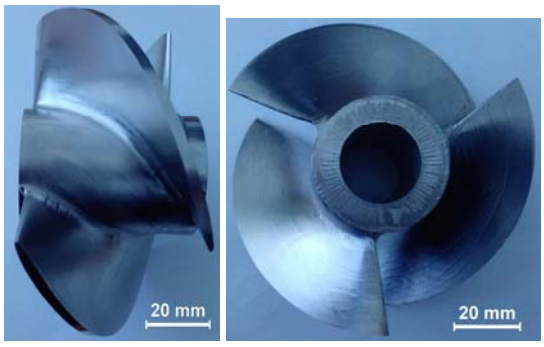

Fig. 1 – Side view (left) and top view (right) of the manufactured model inducer with three blades.

$$rv_u = \frac{RV_u}{R_{ref}U_{ref}},\ x^* = \frac{x - x_{LE}}{x_{TE} - x_{LE}},\ x = \frac{X}{R_{ref}}, \qquad (1)$$

where the reference velocity is $U_{ref} = \omega R_{ref} = 15.64$ m/s, x_{LE} dimensionsionless abscisa at the leading edge (LE) and x_{TE} dimensionsionless abscissa at the trailing edge (TE), respectively. This solution was numerically analyzed [14] and experimentally investigated together with model impeller leading to improved cavitational behavior over an operating range extended up to 20% [15]. This inducer (called "initial") was designed taking into account the suggestions provided by Ashihara et al. [9–11].

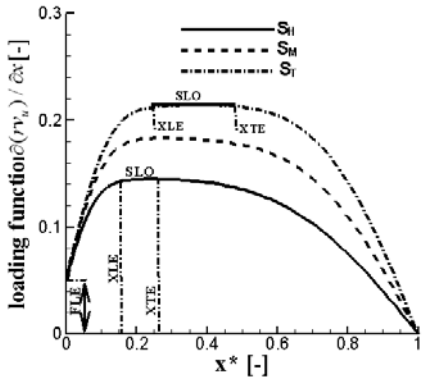

Fig. 2 – Streamline blade loading function along to the three sections (S_H, S_M and S_T) for the initial inducer.

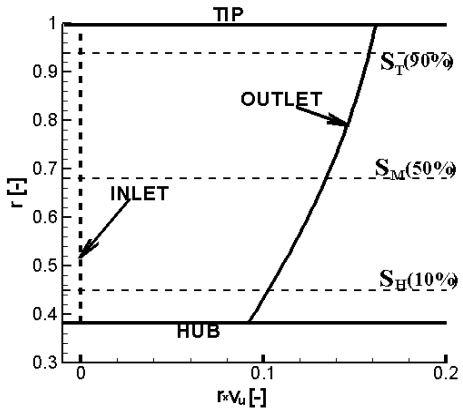

Fig. 3 – Dimensionless moment of momentum at the outlet section of the inducer.

An optimization procedure is developed in this paper and it is applied to the model inducer in order to achieve improved cavitational performances. Section 2 presents the three-dimensional inviscid flow analysis on the initial inducer considering negligible blades thickness. Firstly, a short review of the designing method for thin blade cascades is presented in Section 3. Also, a new analytical parameterized expression for the loading function shape is introduced as a key ingredient in this optimization procedure. Secondly, the optimization steps and the objective function are presented and applied for initial inducer in Section 4. Next, the optimized pressure coefficient obtained on three sections of the inducer blade is compared against 3D numerical results in Section 5 in order to assess the cavitational improvements. Finally, the conclusions are drawn in last section.

2. THREE-DIMENSIONAL FLOW ANALYSIS

The initial inducer model case is designed using [16] with constant thickness of 3 mm and rounded leading and trailing edges, respectively. The 3D inducer blade shape is generated stacking several 2D stream surface profiles [17]. For such profiles, a camber line and thickness representation is used in which a thickness distribution is superimposed on the mean camber line as shown in [19, Fig. 3]. In this representation, the camber line and the thickness distribution can be varied independently leading to a good

control for both parameters. Particularly, the hydrodynamic performances of the inducer are given by the camber line while the blade thickness is selected based on structural considerations. Therefore, throughout this paper the blade thickness is considered negligible. The 3D computational domain includes only one inter-blade channel, Fig. 4, since the flow is similar on each channel at design operating point. The computational domain is extended upstream from leading edge with one cascade pitch while twice the pitch extension is considered downstream from trailing edge. Two camber surfaces corresponding to consecutive blades together with periodic surfaces define the computational domain. A structured mesh with H topology [20] having 420k hexahedral cells was generated using Gambit [21]. The 3D inviscid flow is computed using FLUENT code [22] with following boundary conditions: i) uniform axial velocity on the inlet surface; ii) radial equilibrium condition on the outlet surface; iii) periodic condition on periodic surfaces and iv) impenetrable condition on the chamber, hub and tip surfaces, respectively. Also, the rotational speed of 2900 rpm is imposed on the domain and water is selected as working fluid. As a result, the 3D hydrodynamic field is obtained. The pressure coefficient defined in (2) distribution versus normalized abscissa along to three sections on the inducer blade is plotted in Fig. 5.

$$c_p = \frac{p - p_{IN}}{\frac{1}{2}\rho U_{ref}^2}, \tag{2}$$

where the water density is 998.2 kg/m^3 and the reference static pressure is computed as mass weighted average value on the inlet surface.

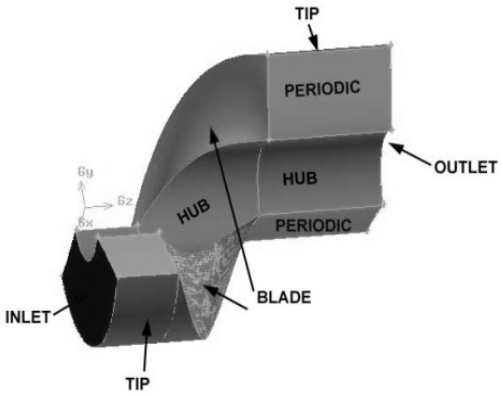

Fig. 4 – 3D computational domain and boundary conditions for initial inducer with thin blades

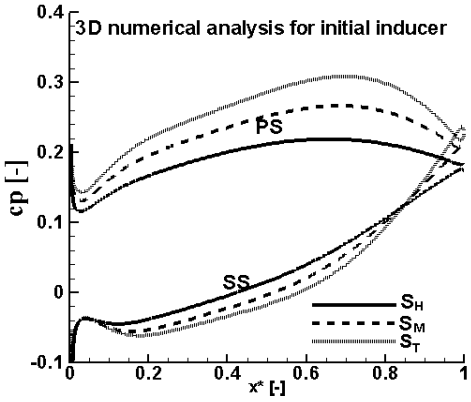

Fig. 5 – Pressure coefficient distribution vs. normalized axial coordinates along to three sections on the inducer thin blade

One can observe in Fig. 5 that the minimum value of pressure coefficient is located on the suction side, in the neighborhood of tip blade at 15% near the leading edge. A general view reveals that the minimum value of the pressure coefficient on each section has quite the same value and it is located in the same region. The last observation proves that the inducer design is quite good even within this trial and error framework.

3. DESIGN OF THIN HYDROFOIL CASCADES

It was already mentioned, the camber surface of each blade is built stacking several camber lines located from hub to tip at different radii (Fig. 6a). Thereby, a thin hydrofoil cascade is obtained at each radius if the camber surface is cut by cylinder (Fig. 6c). As a result, several thin hydrofoil cascades have to be designed at various radii in order to obtain the camber surface of the blade inducer. The design of thin hydrofoil cascades was tackled during last four decades. Hawthorne et al. [22] have proposed a quasi-analytical method for designing two-dimensional highly loaded cascades. Susan-Resiga et al. [23] have developed an analytical solution and applied for optimization the turbines hydrofoil cascades [24]. Further, a synopsis view of the analytical solution is revised together with it assumptions. The fluid is assumed to be incompressible and inviscid and the blades with negligible thickness. Considering a potential flow through the cascade, one assumes that the thin blades may be represented by bound vortices of strength $\gamma(x)$

distributed along camber lines given by $y - f(x) = 0,\ \pm s,\ \pm 2s, \cdots$, where $s = S/L$ is the dimensionless blade pitch, Fig. 6. All lengths are made dimensionless by the cascade axial extent.

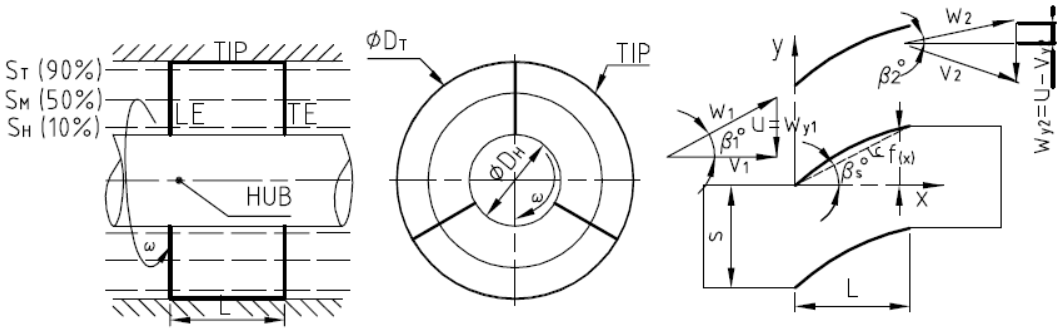

Fig. 6. – The flow through an axial inducer and associated hydrofoil cascade.

The goal of the cascade design is to find the camber line shape $f(x)$ given the flow direction far upstream, β_1, and downstream, β_2, as well as the vortex strength distribution $\gamma(x)$. The axial symmetry assumption requires the pitch-averaged velocity defined according to eq. (3)

$$\bar{W}(x) = \frac{1}{s}\int_0^s W(x,y)\,\mathrm{d}y, \tag{3}$$

while the velocity upstream and downstream the cascade is $\bar{\mathbf{W}}_1$ and $\bar{\mathbf{W}}_2$, respectively,

$$\bar{W}_{x1} = \bar{W}_{x2} = \bar{W}_x, \text{ and } \bar{W}_{y2} - \bar{W}_{y1} = \frac{1}{s}\int_0^1 \gamma(x)\,\mathrm{d}x. \tag{4}$$

Obviously, for blades with zero thickness the pitchwise mean value of the axial velocity remains constant within the bladed region as well. It is introduced the pitchwise averaged boundary vorticity,

$$\bar{\gamma}(x) \equiv \frac{\gamma(x)}{s} = \frac{\mathrm{d}\bar{W}_y}{\mathrm{d}x} \tag{5}$$

and the pitch-averaged tangential velocity is written as follow

$$\bar{W}_y(x) = \bar{W}_{y1} + \int_0^x \bar{\gamma}(t)\,\mathrm{d}t, \text{ or } \bar{W}_{y2} - \bar{W}_{y1} = \int_0^1 \bar{\gamma}(t)\,\mathrm{d}t. \tag{6}$$

One can see from (5) that for cascade design can be alternatively provided by $\bar{W}_y$ schedule instead of $\bar{\gamma}$. An average streamline, starting at origin, can also be found as,

$$\bar{f}(x) = \int_0^x \bar{W}_y(t)\,\mathrm{d}t. \tag{7}$$

Integral equation for the camberline shape can be written

$$\frac{\mathrm{d}f}{\mathrm{d}x}(x) = \frac{1}{2}\left(\frac{\bar{W}_{y1}}{\bar{W}_x} + \frac{\bar{W}_{y2}}{\bar{W}_x}\right) + \frac{1}{\bar{W}_x}\int_0^1 \frac{\bar{\gamma}(t)}{2}\frac{\sinh(2\pi/s)(x-t) + f'(x)\sin(2\pi/s)\left[f(x)-f(t)\right]}{\cosh(2\pi/s)(x-t) - \cos(2\pi/s)\left[f(x)-f(t)\right]}\,\mathrm{d}t. \tag{8}$$

By writing the integrand in (7) as $\frac{\bar{\gamma}(t)}{2}\frac{s}{2\pi}\frac{\mathrm{d}}{\mathrm{d}x}\ln\left\{\cosh(2\pi/s)(x-t) - \cos(2\pi/s)\left[f(x)-f(t)\right]\right\}$, one can integrate (8). If $f = 0$ at the leading edge $x = 0$, i.e. the camberline starts at the origin, we obtain

$$f(x)=\frac{x}{2}\left(\frac{\bar{W}_{y1}}{\bar{W}_x}+\frac{\bar{W}_{y2}}{\bar{W}_x}\right)+\frac{s}{4\pi}\int_0^1\frac{\bar{\gamma}(t)}{\bar{V}_x}\ln\left\{\frac{\cosh(2\pi/s)(x-t)-\cos(2\pi/s)\left[f(x)-f(t)\right]}{\cosh(2\pi/s)t-\cos(2\pi/s)f(t)}\right\}\mathrm{d}t. \tag{9}$$

The determination of the blade profile $f(x)$ requires the integration of equations (8) and (9), each of which has a singularity at $t=x$. As $t\to x$, we have $f(x)-f(t)\to(x-t)f'(x)$ and it can separated the integrand singularities. With $\bar{W}_x=1$, we can rewrite (9) as,

$$\frac{\mathrm{d}f}{\mathrm{d}x}(x)=\frac{\tan\beta_1+\tan\beta_2}{2}+\int_0^1 F_1(x,t)\,\mathrm{d}t+\frac{s\bar{\gamma}(x)}{2\pi}\ln\frac{x}{1-x}, \tag{10a}$$

where

$$F_1(x,t)=\frac{\bar{\gamma}(t)}{2}\frac{\sinh(2\pi/s)(x-t)+f'(x)\sin(2\pi/s)\left[f(x)-f(t)\right]}{\cosh(2\pi/s)(x-t)-\cos(2\pi/s)\left[f(x)-f(t)\right]}-\frac{s\bar{\gamma}(x)}{2\pi}\frac{1}{x-t}. \tag{10b}$$

Now the integrand F_1 vanishes as $t\to x$ and the integral can be calculated with standard quadrature rules. The last term in the right-hand side of (10a) is the Cauchy principal value of the singularity integral. The same approach can be used to remove the singularity in (9),

$$f(x)=x\frac{\tan\beta_1+\tan\beta_2}{2}+\int_0^1 F_2(x,t)\,\mathrm{d}t+\frac{s\bar{\gamma}(x)}{2\pi}\left[\ln\left(\frac{2\pi}{s}\right)+\frac{1}{2}\ln\left(\frac{1+f'^2(x)}{2}\right)+x\ln x+(1-x)\ln(1-x)-1\right], \tag{11a}$$

$$F_2(x,t)=\frac{s\bar{\gamma}(t)}{4\pi}\ln\left\{\frac{\cosh(2\pi/s)(x-t)-\cos(2\pi/s)\left[f(x)-f(t)\right]}{\cosh(2\pi/s)t-\cos(2\pi/s)f(t)}\right\}-\frac{s\bar{\gamma}(x)}{4\pi}\ln\left\{\left[(2\pi/s)(x-t)\right]^2\frac{1+f'^2(x)}{2}\right\}. \tag{11b}$$

The equations (10) and (11) are solved in [23] assuming a first guess for the unknown function $f(x)$ and its derivative $f'(x)$, then the right-hand side is evaluated. A suitable first guess is provided by the average streamline (7). The new values for $f(x)$ and $f'(x)$ are further used to evaluate again the right-hand sides in (10a) and (11a), and the iterative process continues until the solution change from one iteration to the next one is smaller than a given threshold. Since the integrals of F_1 and F_2 cannot be evaluated analytically, a discrete representation of the unknown function was considered by Susan–Resiga et al. [23]. First, a set of points $0=x_1<x_2<\ldots<x_{n+1}=1$ are considered on the unit interval. The goal was to find the function values $f_1\equiv f(x_1)$, $f_2\equiv f(x_2)$, $\ldots, f_{n+1}\equiv f(x_{n+1})$ as well as the function derivatives $f'_1\equiv f'(x_1)$, $f'_2\equiv f'(x_2)$, .., $f'_{n+1}\equiv f'(x_{n+1})$ using the above iterative method.

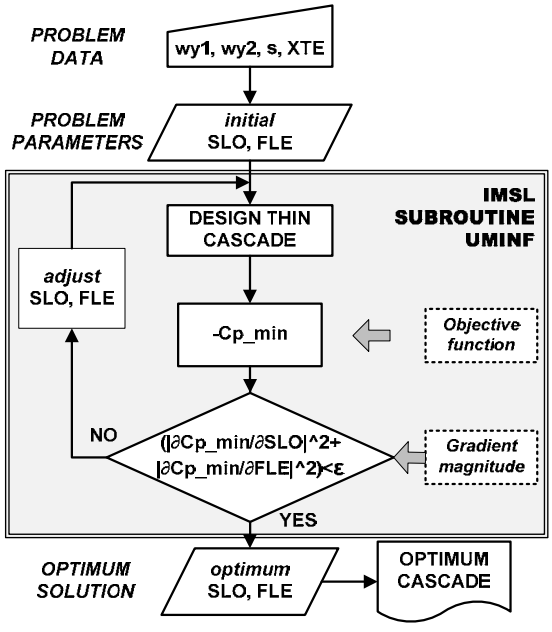

Fig. 7 – Flow chart of the optimization procedure.

The key ingredient of the design and optimization procedure of the thin hydrofoil cascade is

the vortex strength distribution $\overline{\gamma}(x)$ defined on the unit interval. A new loading function shape $g(x, XTE, SLO, FLE)$ with three parameters is introduced by eq. (12): 1) the abscissa, XTE; 2) the slope SLO; and 3) the load (Fig. 2) at the leading edge, FLE ($\overline{\gamma}(0) = FLE$).

$$g(x, \mathrm{XTE}, \mathrm{SLO}, \mathrm{FLE}) = (\mathrm{FLE} + \mathrm{SLO} \cdot x)\,\mathrm{erf}\left(\frac{\sqrt{\pi}}{2} \cdot \frac{1-x}{1-\mathrm{XTE}}\right) \cdot g^{\otimes}(\mathrm{XTE}, \mathrm{SLO}, \mathrm{FLE}), \tag{12}$$

where $g^{\otimes}(\mathrm{XTE}, \mathrm{SLO}, \mathrm{FLE}) = \left\{\int_0^1 (\mathrm{FLE} + \mathrm{SLO} \cdot x)\,\mathrm{erf}\left(\frac{\sqrt{\pi}}{2} \cdot \frac{1-x}{1-\mathrm{XTE}}\right)\mathrm{d}x\right\}^{-1}$

resulting in

$$\int_0^1 g(x, \mathrm{XTE}, \mathrm{SLO}, \mathrm{FLE})\,\mathrm{d}x = 1.$$

The new function of loading shape is defined in terms of three parameters (*XTE*, *SLO* and *FLE*) while an expression with two parameters was used by Resiga et al. [23]. The third parameter *FLE* is directly linked with the camber line curvature at the leading edge. As a result, the camber line curvature at the leading edge is decreased if the load value at leading edge is larger.

4. OPTIMIZATION PROCEDURE

The parametric camber line is integrated in the optimization procedure in order to be found the minimum value of the objective function. The quasi-Newton method and a finite-difference gradient are used to minimize the function with respect to both parameters SLO and FLE. This optimization procedure is effective if the problem is not noisy [25]. As a result, the gradients are found relatively easily and only a local search is required. The optimization algorithm, shown in Fig. 7, is implemented in FORTRAN using the UMINF subroutine from IMSL library [26]. The optimization procedure is applied for several thin hydrofoil cascades with prescribed values of w_{y1}, w_{y2}, and s given in Table 2. Each thin hydrofoil cascade was computed imposing the normalized abscissa XTE yielding the parameters slope SLO and loading at the leading edge FLE as well as the minimum value of the pressure coefficient cp_{min}. The procedure is applied for several thin hydrofoil cascades associated to different sections from hub to tip with variable values of the normalized abscissa XTE.

Table 2

Optimised design parameters of the cascades

section	S_H	S_M	S_T
$w_{y1} = W_{y1}/W_{x1}$	1.2941	1.9448	2.6318
$w_{y2} = W_{y2}/W_{x2}$	0.6591	1.3959	2.1603
$s = S/L$	0.9674	1.4539	1.9674
XTE	0.27	0.465	0.59
SLO	0.12005	0.0645	0.04804
FLE	0.3681	0.2993	0.2489

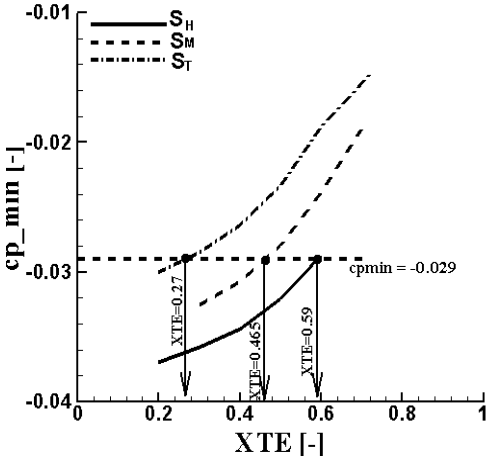

Fig. 8 – The distribution of the minimum value of pressure coefficient computed for several hydrofoil cascade on the sections: S_H (solid line), S_M (dashed line), S_T (dash dot line).

The distribution of the minimum pressure coefficient in terms of the normalized abscissa XTE on three sections, near the hub (S_H), middle (S_M) and tip (S_T) are plotted in Fig. 8.

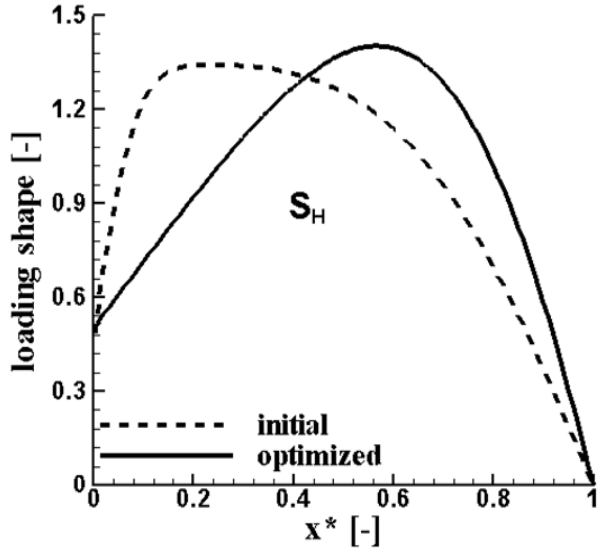

Fig. 9 – The loading shape distribution on the section S_H near the hub: initial (dash line) and optimized (solid line).

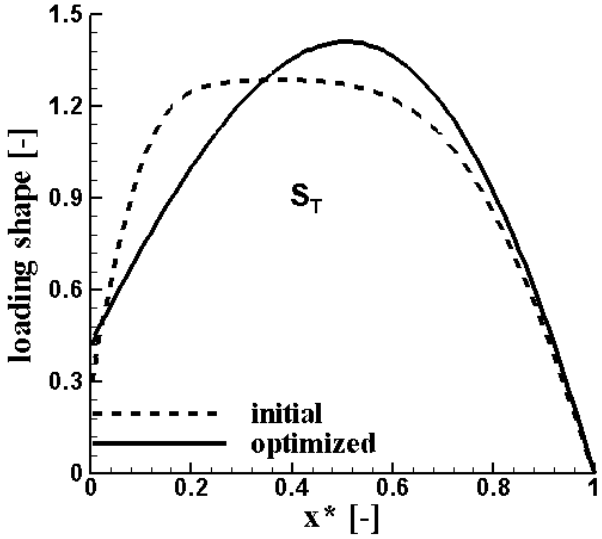

Fig. 10 – The loading shape distribution on the section S_T near the tip: initial (dash line) and optimized (solid line).

The optimum value of the normalized abscissa is obtained for each section imposing the minimum pressure coefficient value (e.g. cp_{min}= – 0.029) selected based on the problem requirements. Then the optimum thin hydrofoil cascades are obtained (Table 2) leading to the chamber surface of the blade. Consequently, the same value of the minimum pressure coefficient is obtained along to the camber surface of the inducer.

The initial and optimized loading shapes on the sections S_H and S_T are shown in Figs. 9 and 10, respectively. One can see that the maximum load of the optimized shape is shifted toward the trailing edge whilst the load at leading edge (FLE value) is increased in order to reduce the curvature of the chamber line.

5. NUMERICAL RESULTS

The pressure coefficient distribution on optimized thin hydrofoil cascade of the pump inducer at three sections S_H, S_M and S_T is plotted in Fig. 11. A wide flat region at –0.029 can be observed in the optimized pressure coefficient distribution on the suction side at all sections leading to an improved cavitational behavior of the pump inducer. The optimized pressure coefficient distribution is compared with initial one (plotted in Fig. 5) in order to assess the improvements. One can see that on the section S_H near the hub the minimum value is increased from – 0.046 to – 0.029 (Fig. 12) while on section S_T near the tip from – 0.060 to – 0.029 (Fig. 13), respectively. Additionally, the position of the minimum value is shifted from x^*= 0.11 to x^*= 0.39 on section S_H and on the section S_T from x^*= 0.285 to x^*= 0.33. It is clearly shown that the optimization procedure shifts the minimum value of the pressure coefficient toward the middle region of the inducer camber surface.

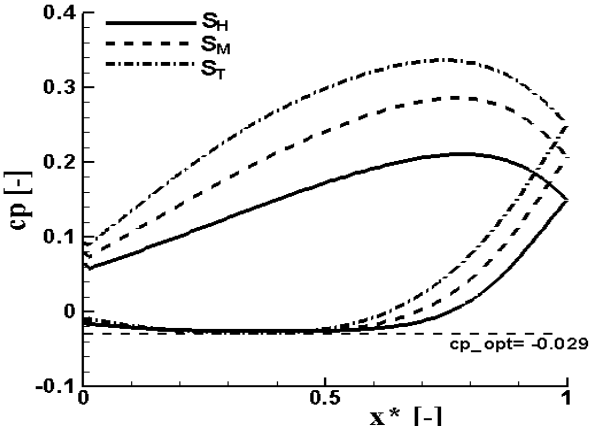

Fig. 11 – Optimized pressure coefficient distribution on the inducer: S_H (solid line), S_M (dashed line), S_T (dash-dot line).

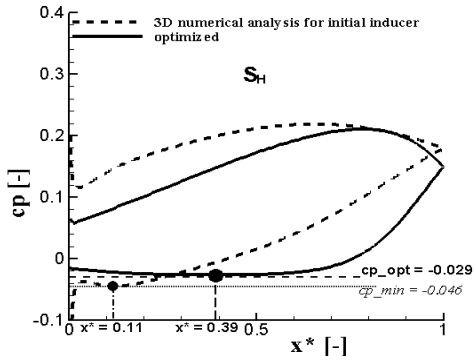

Fig. 12 – Pressure coefficient distribution on the section S_H near the hub: initial (dash line) and optimized (solid line).

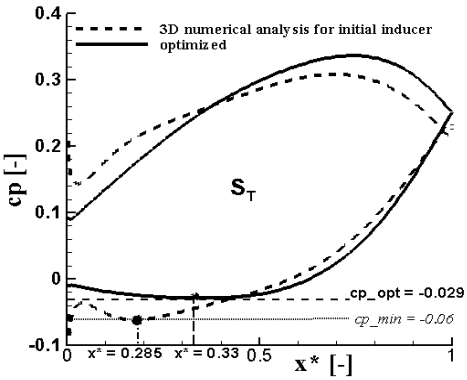

Fig. 13 –Pressure coefficient distribution on the section S_T near the tip: initial (dash line) and optimized (solid line).

6. CONCLUSIONS

In this paper, a new procedure based on inverse design method was developed to optimize the cavitational behavior of the pump inducer. We prescribe an axial inflow with an outlet swirl suited for the pump impeller inlet. Firstly, the 3D inviscid flow analysis of the inducer with thin blades is performed. Secondly, several thin hydrofoil cascades are optimized based on cavitation criterion but the results are only presented for three of them. The key ingredient in optimization procedure is the new function of loading shape with three parameters introduced in this paper. This function provides an appropriate mathematical model for the distribution of loading from leading edge to trailing edge on each blade section. The procedure is applied for pump inducer with three blades in order to obtain optimized cavitational performances. The numerical value of the minimum pressure coefficient for the optimized case leads to an improved cavitational behavior of the pump inducer. Also, the optimization procedure shifts the minimum value of the pressure coefficient toward the middle region of the inducer chamber surface.

ACKNOWLEDGEMENTS

Ms. Moisa I.G. was partially supported by the strategic grant POSDRU 2009 project ID 50783 of the Ministry of Labour, Family and Social Protection, Romania, co-financed by the European Social Fund – Investing in People. Prof. Susan-Resiga R. and Dr. Muntean S. were supported by the Romanian Academy program "Hydrodynamics Optimization and Flow Control of the Hydraulic Turbomachinery in order to improve the Energetic and Cavitational Performances".

REFERENCES

1. U.S. DEPARMENT OF ENERGY (DOE), *Variable Speed Pumping – A Guide to Successful Applications. Executive Summary*, Technical Report DOE/GO-102004-1913, April 2004.
2. U.S. DEPARMENT OF ENERGY (DOE), *Energy Efficiency and Renewable Energy*, *Improving Pumping System Performance – A Sourcebook for Industry*, 2nd ed., May 2006.
3. Anton, I., *Cavitation* (in Romanian) Romanian Academy Publishing House, 2, 1985.
4. Anton, L.E., and Miloş, T., *Centrifugal pumps with inducers* (in Romanian), Orizonturi Universitare Publishing House, Timişoara, 1998.
5. Anton, L.E., Stuparu, A., Baya, A, *Numerical and Experimental Investigations of the Flow into an Inducer*, Proc. of the International Conference on Hydraulic Machinery and Equipments, October 16-17, Timişoara, 2008, pp. 1–6.
6. Stuparu, A., Muntean, S., Anton, L.E., *Validation of the Two-dimensional Numerical Investigation Methodology of the Turbulent Flow into an Inducer with the Three-dimensional Computation*, Proc. of the 14th International Conference on Fluid Flow Technologies, September 9-12, Budapest, Hungary, **2**, 2009, pp. 736–742.
7. Brennen, C., *Hydrodynamics of pumps*, Oxford University Press, 1994.
8. Zangeneh, M., Goto, A., Harada, H., *On the role of three-dimensional inverse design methods in turbomachinery shape optimization*, Proc. of the Institution of Mechanical Engineers, Part C: Journal of Mechanical Engineering Science, **123**, *1*, pp. 27–42, 1999.

19. Ashihara, K., Goto, A., Kamijo, K., Yamada, H., Hashimoto, T., Uchiumi, M., *Study on Turbopump Inducers Designed by Inverse Design Method*, Proc. of the 1st International Symposium on Advanced Fluid Information, October 4–5, Sendai, Japan, 2001, pp. 1–6.
10. Ashihara, K., Goto, A., Kamijo, K., Yamada, H., Uchiumi, M., *Improvements of Inducer Inlet Backflow Charactheristics using 3D inverse design method*, AIAA 2002-4158, 2002, pp. 1–9.
11. Ashihara, K., Goto, A., *Effects of blade loading on pump inducer performance and flow fields*, Proc. of ASME 2002 Fluids Engineering Division Summer Meeting, July 14–18, Montreal, Canada, 2002, pp. 1–10.
12. Anton, A., *In situ performance curves measurements of large pumps*, IOP Conf. Ser.: Earth Environ. Sci., **12**, 2010. 012090.
13. Moisa, I.G., Stuparu, A., Susan-Resiga, R.F., Muntean, S., *Inverse Design of a Pump Inducer and Performance Evaluation with 3D Flow Simulation*, Proc. of the 4th International Meeting on Cavitation and Dynamic Problems in Hydraulic Machinery and Systems, Belgrade, Serbia, 2011, pp.151–160.
14. Moisa, I.G., Ginga, G., Muntean, S., Susan-Resiga, R.F., *Inverse Design and Three-dimensional Numerical Analysis of the Inducer for Storage Pump Impeller*, Proc. of the 15th International Conference on Fluid Flow Technologies, September 4-7, Budapest, Hungary, **2**, 2012, pp. 812–819.
15. Gînga. G., *Numerical and experimental analysis of the centrifugal storage pump operation* (in Romanian), PhD Thesis, Politehnica University Press, Timişoara, 2012.
16. *** *Advanced design technology, TurboDesign-1 V3.1.*, User's Manual, London, UK, 2009.
17. Miller, P.L., Oliver. J.H., Miller, D.P., Tweedt, D.L., *BladeCAD: An Interactive Geometric Design Tool for Turbomachinery Blades*, NASA Technical Memorandum 107262, 1996.
18. Koini, G.N., Sarakinos, S.S., Nikolos, I.K., *A Software Tool for Parametric Design of Turbomachinery Blades*, Advances in Engineering Software, **40**, *1*, pp. 41–51, 2009.
19. *** *FLUENT INC., GAMBIT 2.4.*, *User's Guide*, Fluent Incorporated, Lebanon, New Hampshire, 2006.
20. Sottas, G., Reymond, J.-D., *Mesh Generation Techniques for Inviscid-Flow Simulation in Turbines*, In Weatherhill N.P., Eiseman P.R., Häuser J., and Thompson J.F. (eds.), *Numerical Grid Generation in Computational Fluid Dynamics and Related Fields*, Pineridge Press Limited, Swansea, U.K., 1994, pp. 653–664.
21. *** *FLUENT INC., FLUENT V6.3, User's Guide*, Lebanon, New Hampshire, 2006.
22. Hawthorne, W.R., Tan, C.S., Wang, C., McCune, J.E., *Theory of Blade Design for Large Deflections: Part I – Two Dimensional Cascades*, ASME Journal of Engineering for Gas Turbines and Power, **106**, pp. 346–353, 1984.
23. Susan-Resiga, R., Muntean, S., Bernad, S., Frunză, T., Balint, D., *The hydrofoil cascade design and numerical flow analysis. Part I – Design*, Proc. of the Romanian Academy, Series A, **7**, *2*, pp. 117–126, 2006.
24. Frunză, T., Susan-Resiga, R., Muntean, S, Bernad, S., *Optimization of the Hydrofoil Cascade and Validation with Quasi-Analytical Solution for Hydraulic Machinery*, IOP Conf. Ser.: Earth Environ. Sci., **12**, 012075, 2010.
25. NATO RTO, *Strategies for Optimization and Automated Design of Gas Turbine Engine*, RTO-EN-AVT-167, 2010.
26. VISUAL NUMERICS, *IMSL Fortran Library User's Guide. Mathematical Functions in Fortran*, 2003.

Received January 15, 2013